Cleaning graphene: comparing heat treatments in air and in vacuum

Mukesh Tripathi, Andreas Mittelberger, Kimmo Mustonen, Clemens Mangler, Jani Kotakoski, Jannik C. Meyer and Toma Susi*

Faculty of Physics, University of Vienna, Boltzmanngasse 5, Vienna, 1090, Austria

Received XXXX, revised XXXX, accepted XXXX
Published online XXXX

Key words: graphene, cleaning, annealing, STEM.

* Corresponding author: e-mail toma.susi@univie.ac.at, Phone: +43-01-4277-72855

Surface impurities and contamination often seriously degrade the properties of two-dimensional materials such as graphene. To remove contamination, thermal annealing is commonly used. We present a comparative analysis of annealing treatments in air and in vacuum, both *ex situ* and *"pre-situ"*, where an ultra-high vacuum treatment chamber is directly connected to an aberration-corrected scanning transmission electron microscope. While *ex situ* treatments do remove contamination, it is challenging to obtain atomically clean surfaces after ambient transfer. However, *pre-situ* cleaning with radiative or laser heating appears reliable and well suited to clean graphene without damage to most suspended areas.

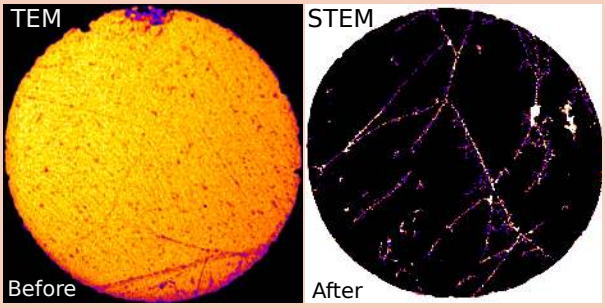

Pre-situ annealing of typical dirty graphene samples yields atomically clean areas several hundred nm^2 in size.

1 Introduction Graphene [1] has attracted considerable attention due to its excellent intrinsic properties, leading to many potential applications including DNA translocation [2], nanoelectronic devices [3], and sensors [4]. Chemical vapor deposition (CVD) allows large area graphene to be synthesized scalably and in high-yield on transition metal surfaces, from which polymers such as poly methyl methacrylate (PMMA) are used to transfer it onto target substrates [5]. To dissolve PMMA after transfer, organic solvents like acetone, chloroform and acetic acid are commonly used [6,7]. However, none of these solvents are able to completely dissolve PMMA, and a thin layer of polymeric residues are left absorbed on the surfaces [8]. This is a major drawback of polymer-assisted transfer and can degrade the electronic properties of graphene by introducing unintentional doping and charge impurity scattering [9]. In addition, hydrocarbon impurities are directly absorbed from the atmosphere onto the surface. Their chemical nature is still not precisely known, but most studies point to (-CH_2-) and (-CH_3-) groups [10]; carboxyl, methoxy and sp^3-hybridized carbon [11–13]; and (C = O) functional groups [14]. Finally, mobile contamination may be pinned into place by the electron beam [15]. Contamination makes atomic level characterization by electron microscopy and electron energy loss spectroscopy [16] difficult, not to mention more ambitious goals such as single-atom manipulation [17,18].

To clean graphene, several methods have been reported. Conventional thermal annealing is optimized by varying the treatment temperature in air [13,19], in vacuum [6,9,20,21] and in gas environments such as Ar/H_2 [22,12], CO_2 [23] or N_2 [24]. Moreover, vacuum annealing at higher temperature for shorter times, i.e. rapid-thermal annealing [24], has been successfully used to remove surface contamination. Several other approaches such as dry-cleaning with activated carbon [14],

wet chemical treatment using chloroform [6], and deposition of metal catalyst and subsequent annealing [25] have been studied. However, adsorbents or chemicals also leave residues, and depositing metal will affect transport and other properties. Non-chemical routes such as mechanical cleaning using contact mode atomic force microscopy [26] or plasma treatment [27] have limited ability to remove contamination over large areas.

In this work, we analyze and compare the effectiveness of heat treatments in air and in vacuum to clean graphene. We investigate its relative cleanliness after *ex situ* annealing in air on a hot plate or in a vacuum chamber. We further demonstrate a new, effective and reliable cleaning approach using black body radiative or laser-induced heating in vacuum. In this "*pre-situ* cleaning", the sample is annealed in the same vacuum system as the characterization equipment, to which it is transferred without exposure to the ambient. While this is a standard technique for surface science, it has until now not been possible to combine it with electron microscopy. To study the effectiveness of the methods used, our samples were characterized using low acceleration voltage transmission electron microscopy (TEM) and atomic resolution aberration-corrected scanning transmission electron microscopy (STEM).

We find that while *ex situ* treatments do remove some contamination, when effective they also cause significant damage. Only with the *pre-situ* method was it possible achieve large areas of atomically clean graphene.

2 Experimental Commercially available CVD-grown monolayer graphene transferred onto Quantifoil TEM grids without the use of polymer (Graphenea Inc.) was used for the experiments. All *ex situ* samples were characterized using a bench-top low acceleration voltage transmission electron microscope (LVEM5, 5 kV). Selected *ex situ* and all *pre-situ* samples were characterized at high resolution using the aberration-corrected scanning transmission electron microscope Nion UltraSTEM100 operated at 60 kV (with a standard 12 h 130 °C vacuum bake before insertion into the microscope, apart from the radiatively heated samples inserted via a separate airlock).

Darker contrast in our bright-field (TEM) images indicates greater scattering and thus greater thickness of the material. In dark-field (STEM) images, the contrast is reversed due to the annular dark field detection of scattered instead of transmitted intensity. The contrast is therefore a direct measure of the amount of contamination overlying the atomically thin graphene sheets. All presented images have been treated with a Gaussian filter and colored with the ImageJ lookup table "fire" to highlight relevant details.

We used two *ex situ* cleaning techniques: air and vacuum annealing. In air, samples were heated on a hot plate between 300–500 °C for times ranging from 15 min to 1 h. Vacuum annealing was carried out in a vacuum evaporator at a pressure of 10^{-6} Torr (Korvus Technology). TEM grids were inserted into the vacuum chamber in a ceramic bucket wrapped with a resistive coil and a thermocouple placed inside to measure the temperature.

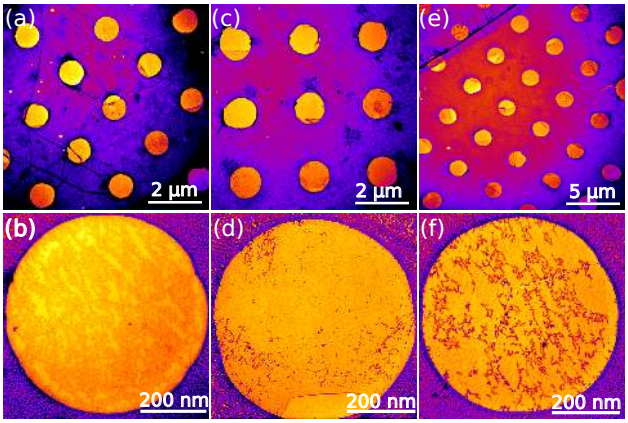

Figure 1 TEM images of graphene after heat treatment in air. (a) Overview and (b) magnified view after annealing at 400 °C for 1 h. (c) Overview and (d) magnified view after 450 °C for 30 min. (e) Overview and (f) magnified view after 500 °C for 15 min.

For *pre-situ* annealing, we likewise used two techniques: radiative heating and laser annealing. The vacuum level for both *pre-situ* methods was $\sim 10^{-8}$ Torr, and the samples were transferred for imaging into the Nion UltraSTEM without exposure to air. Radiative heating was effected by a tungsten (W) wire that can be resistively heated to high temperatures, mounted in a vacuum chamber attached to the microscope. Distance between the wire and sample was ∼2–3 mm and the treatment time 15 min. The wire power was iteratively increased until cleaning was observed, yielding good results for a current of 7 A, corresponding to a thermal power of 64 W and a wire temperature of ∼1750 K.

For laser annealing, a high power diode laser (445 nm, tunable up to 6 W, Lasertack GmbH) was aimed through a viewport at the sample held in the parked pneumatic transfer arm. The samples were again iteratively treated with increasing laser power until cleaning was observed, leading to good results with 600 mW (10 % duty cycle) for 2 min. The laser spot was ∼1 mm^2 in size and the distance between the laser source and sample was ∼40 cm. Although it is difficult to precisely estimate the heating caused by the laser, by assuming that about 20% of its power is deposited on the sample, that the coupling to the sample holder is relatively poor, and that the system reaches a thermal equilibrium of absorption and emission, we can estimate a temperature of around 1100–1300 °C. At higher power the laser was observed to destroy the sample; since the melting point of the gold support is 1100 °C, it appears that our optimum is close to this limit.

3 Results and discussion Figure 1 shows low voltage TEM images of suspended monolayer graphene after annealing in air at temperatures between 400–500 °C

(treatment at lower temperatures does not yield larger clean areas, even if contamination layers are thinner). After air treatment at 400 °C for 1 h, structural damage of graphene starts to emerge, but residues have not been much affected as shown in Fig. 1a and b. By increasing the temperature to 450 °C for 30 min, tearing of graphene sheets becomes more frequent and the concentration of impurities is reduced as illustrated in Fig. 1c and d. However, significant contamination still remains. At 500 °C for 15 minutes, crack formation is common almost everywhere on the sample, while the density of residues decreases further as shown in Fig. 1e and f. At the same time, some regions of the contamination yield a greater scattering intensity after the treatment, which indicates greater local thickness. A two-step treatment of washing the sample with aqueous acetonitrile and baking in air did not show additional effect. Thus, air annealing at high temperatures does help in removing residues, but severe damage occurs [28] in the suspended graphene regions, presumably assisted by the etching of grain boundaries.

In vacuum, graphene can withstand significantly higher temperatures [21,29], but cleaning is also expected to be slower without a reactive atmosphere. Fig. 2 shows TEM and STEM images of graphene annealed between 600–750 °C (heated at a rate of 10 °C/min and cooled to room temperature in N_2). The TEM images in Fig. 2a of a sample heated to 600 °C show that contaminants are covering the surface, with small clean spots no larger than a few tens of nm^2. After thermal treatment at 650 °C for 15 min, surface contamination was reduced (Fig. 2b). However, long treatments at high temperature start to cause crack formation even in vacuum. We further increased the annealing temperature to 750 °C but reduced the time to only 3 min, and observed that many contaminants had been removed (Fig. 2c). We also found apparently almost fully clean areas, apart from some remaining chains of impurities as shown in Fig. 2c (probably due to greater binding of impurities at wrinkles or grain boundaries). However, even this short treatment resulted in severe tearing of the suspended graphene. While chemical etching should be suppressed in vacuum, the mismatch in the coefficients of thermal expansion of graphene [30] and the gold substrate [31] causes a mechanical stress of $\sim$1.7% at this temperature that may contribute to the observed damage.

To verify the cleaning, we imaged the 750 °C sample at higher resolution in the STEM. The medium angular annular dark field (MAADF) image of Fig. 2d includes both large clean-looking areas and chain-like impurity patterns. Since STEM contrast is directly proportional not only to the number of atoms in the beam path but also their atomic number [32], the bright spots are possibly heavier elements such as particles of gold from the support grid that have become mobile at high temperatures. At higher magnifications, we observed that a thin layer of contamination is still covering the regions that appear clean at lower resolution. Furthermore, the square bright contrast in Fig. 2e was

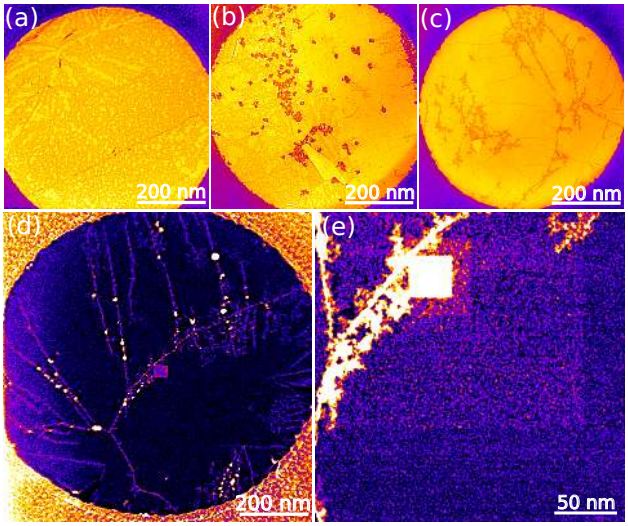

Figure 2 TEM and STEM images of graphene after vacuum annealing. (a) 600 °C for 30 min, (b) 650 °C for 15 min, (c) 750 °C for 3 min. After annealing at 750 °C, this sample was transferred via ambient to the Nion UltraSTEM. (d) Low magnification STEM image and (e) magnified view of a clean-looking area, revealing that a layer of contamination still covers the surface, and more rapidly accumulates under the beam (bright squares).

caused by mobile contamination pinned onto the surface by the electron beam. These findings may be explained by the highly lipophilic nature of graphene: a thin layer of contamination quickly adsorbs on the surface when graphene is exposed to the ambient [33]. Alternatively, the contaminants may not be desorbed by this vacuum treatment, but merely swept aside into larger aggregates (which would explain the enhanced contrast at the chain-like impurity patterns), only to diffuse back afterwards.

To quantify the effect of cleaning, in Fig. 3 we plot the integrated intensity measured over several hundred nm^2 of graphene (divided by the intensity measured over vacuum to normalize for differences in beam focusing) for air and vacuum annealing at different temperatures. For both treatments, the integrated intensity approaches a value close to unity with increasing temperature, indicating a decrease of impurity concentration as contaminants on the surface diffuse away or are desorbed. Since we used different treatment times at different temperatures, to compare the treatments we also calculate the time integral of the thermal energy per mole defined as

$$S_{th} = N_{\mathrm{A}} k_{\mathrm{B}} T t, \tag{1}$$

where N_{A} is the Avogadro constant, k_{B} the Boltzmann constant, T the temperature in Kelvin, and t the treatment time. From the plot of this figure of merit against the normalized intensity in Fig. 3 we see that relatively shorter treatments are required at higher temperature for the same or even better cleaning effect. This corroborates the effectiveness of rapid-thermal annealing.

To clean graphene using *pre-situ* annealing in a custom-built vacuum chamber attached to the STEM column, we made use of both radiative energy transfer from a resistively heated W wire and from a high power laser aimed at the sample. In both cases the sample was transferred for observation without breaking the vacuum. The MAADF images in Fig. 4a and b show graphene after W wire heating, and the results of the laser cleaning are shown in Fig. 4c and d. The cleaning effect is similar for both pre-situ treatments: despite structural damage to some suspended areas, surface contaminants are greatly reduced and large uniformly clean graphene regions of several hundred nm^2 are obtained (the MAADF image in Fig. 4e shows an example of the atomically clean lattice).

To estimate the amount of damage, we counted the number of broken suspended graphene areas (some are damaged also in untreated samples). These were increased by more than two-fold for all of our cleaning methods, pre-situ ones having the smallest increase (presumably due to the best vacuum conditions). Nonetheless, especially in the *pre-situ* samples, it was easy to find clean and fully intact areas. Interestingly, while we observed mobile contamination pinning under the beam in these samples, in most cases this occurred only when the field of view contained pre-existing contamination or other defects.

4 Conclusions In conclusion, we have compared heat treatments to clean graphene in air and in vacuum. We show that air annealing is not a good method: contamination remains on the surface, and severe damage occurs at higher temperatures where the treatment is more effective. Annealing at even higher temperatures in vacuum is more effective in removing surface contaminants, but some seem to readsorb upon exposure to an air ambient. This issue can be overcome with *pre-situ* annealing via radiative or laser-induced heating in the same vacuum system as the electron microscope. While some structural damage seems unavoidable, these methods appear to be reliable and controllable for cleaning graphene and potentially other 2D crystals. However, caution must be taken in selecting the treatment time and the laser or thermal power to avoid destroying the sample. With optimal parameters, large areas of atomically clean graphene can be easily obtained.

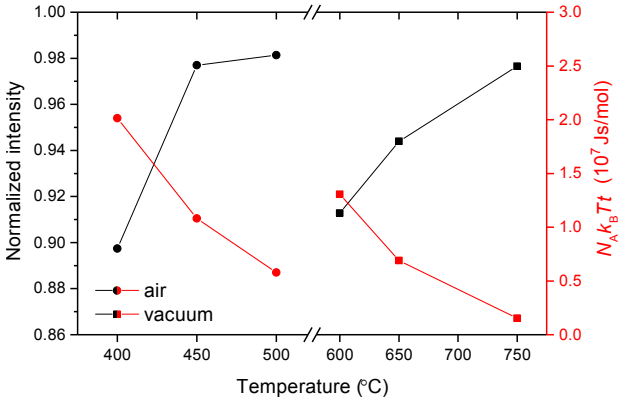

Figure 3 Quantifying the cleaning effect of heat treatments in air and in vacuum. The left axis shows the normalized integrated intensity as a function of annealing temperature (for untreated samples, a typical value was ∼0.61). As the temperature increases, the integrated intensity approaches that of vacuum, corresponding to the reduction of impurities. The right axis shows the thermal energy per mole multiplied by the treatment time (Eq. 1), suggesting that higher temperature treatments are more effective despite shorter treatment times.

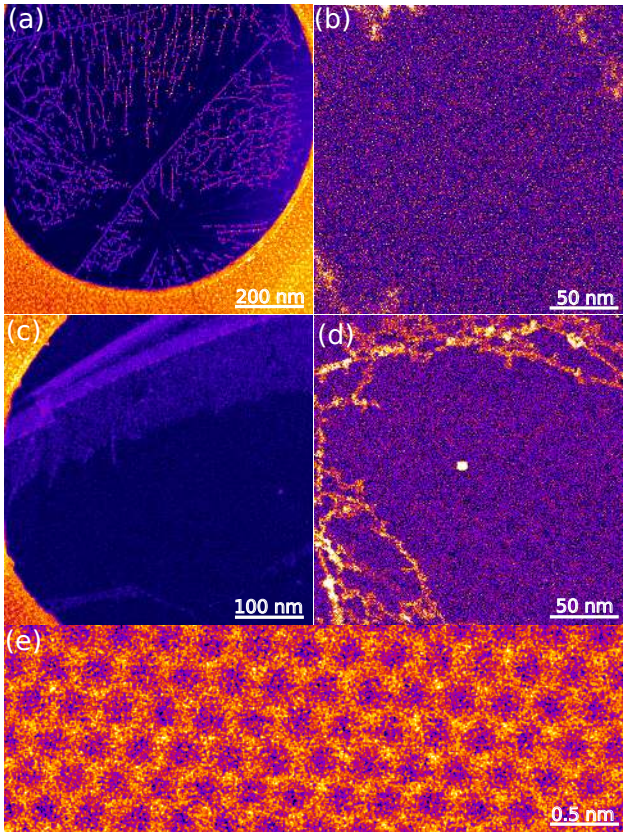

Figure 4 STEM images showing cleaned graphene after *pre-situ* annealing. (a) Low and (b) intermediate magnification images after radiative heating, and (c) low and (d) intermediate magnification images after laser-induced heating in vacuum. Panel (e) shows an example of the atomically resolved and clean graphene lattice (the non-ideal imaging conditions presumably resulted from residual heat from the treatment).

Acknowledgements M.T. and T.S. acknowledge funding by the Austrian Science Fund (FWF) via project P 28322-N36. A.M., K.M., C.M., and J.C.M. were supported by the European Research Council (ERC) Grant No. 336453-PICOMAT. K.M. acknowledges financial support from the Finnish Foundations Post Doc Pool, and J.K. by the Wiener Wissenschafts-, Forschungs- und Technologiefonds (WWTF) project MA14-009.

References

[1] K. S. Novoselov, A. K. Geim, S. V. Morozov, D. Jiang, Y. Zhang, S. V. Dubonos, I. V. Grigorieva, and A. A. Firsov, Science **306**(5696), 666–669 (2004).

[2] C. A. Merchant, K. Healy, M. Wanunu, V. Ray, N. Peterman, J. Bartel, M. D. Fischbein, K. Venta, Z. Luo, A. T. C. Johnson, and M. Drndić, Nano Letters **10**(8), 2915–2921 (2010).

[3] H. A. Becerril, J. Mao, Z. Liu, R. M. Stoltenberg, Z. Bao, and Y. Chen, ACS Nano **2**(3), 463–470 (2008).

[4] F. Schedin, A. K. Geim, S. V. Morozov, E. W. Hill, P. Blake, M. I. Katsnelson, and K. S. Novoselov, Nat Mater **6**(9), 652–655 (2007).

[5] X. Li, W. Cai, J. An, S. Kim, J. Nah, D. Yang, R. Piner, A. Velamakanni, I. Jung, E. Tutuc, S. K. Banerjee, L. Colombo, and R. S. Ruoff, Science **324**(5932), 1312–1314 (2009).

[6] Z. Cheng, Q. Zhou, C. Wang, Q. Li, C. Wang, and Y. Fang, Nano Letters **11**(2), 767–771 (2011).

[7] M. Her, R. Beams, and L. Novotny, Physics Letters A **377**(2122), 1455–1458 (2013).

[8] Y. C. Lin, C. Jin, J. C. Lee, S. F. Jen, K. Suenaga, and P. W. Chiu, ACS Nano **5**(3), 2362–2368 (2011).

[9] A. Pirkle, J. Chan, A. Venugopal, D. Hinojos, C. W. Magnuson, S. McDonnell, L. Colombo, E. M. Vogel, R. S. Ruoff, and R. M. Wallace, Applied Physics Letters **99**(12), 122108 (2011).

[10] Z. Li, Y. Wang, A. Kozbial, G. Shenoy, F. Zhou, R. McGinley, P. Ireland, B. Morganstein, A. Kunkel, S. P. Surwade, L. Li, and H. Liu, Nat Mater **12**(10), 925–931 (2013).

[11] A. Yulaev, G. Cheng, A. R. Hight Walker, I. V. Vlassiouk, A. Myers, M. S. Leite, and A. Kolmakov, RSC Adv. **6**, 83954–83962 (2016).

[12] Y. Ahn, J. Kim, S. Ganorkar, Y. H. Kim, and S. I. Kim, Materials Express **6**(1) (2016).

[13] W. Xie, L. T. Weng, K. M. Ng, C. K. Chan, and C. M. Chan, Carbon **94**, 740–748 (2015).

[14] G. Algara-Siller, O. Lehtinen, A. Turchanin, and U. Kaiser, Applied Physics Letters **104**(15), 153115 (2014).

[15] J. C. Meyer, C. O. Girit, M. F. Crommie, and A. Zettl, Applied Physics Letters **92**(12), 123110 (2008).

[16] T. Susi, T. P. Hardcastle, H. Hofsäss, A. Mittelberger, T. J. Pennycook, C. Mangler, R. Drummond-Brydson, A. J. Scott, J. C. Meyer, and J. Kotakoski, 2D Materials **4**(2), 021013 (2017).

[17] T. Susi, Research Ideas and Outcomes **1**(12), e7479 (2015).

[18] T. Susi, J. Meyer, and J. Kotakoski, Ultramicroscopy **in press** (2017).

[19] X. Wang, A. Dolocan, H. Chou, L. Tao, A. Dick, D. Akinwande, and C. G. Willson, Chemistry of Materials **29**(5), 2033–2039 (2017).

[20] Y. C. Lin, C. C. Lu, C. H. Yeh, C. Jin, K. Suenaga, and P. W. Chiu, Nano Letters **12**(1), 414–419 (2012).

[21] Z. H. Ni, H. M. Wang, Z. Q. Luo, Y. Y. Wang, T. Yu, Y. H. Wu, and Z. X. Shen, Journal of Raman Spectroscopy **41**(5), 479–483 (2010).

[22] W. Choi, Y. S. Seo, J. Y. Park, K. B. Kim, J. Jung, N. Lee, Y. Seo, and S. Hong, IEEE Transactions on Nanotechnology **14**(1), 70–74 (2015).

[23] C. Gong, H. C. Floresca, D. Hinojos, S. McDonnell, X. Qin, Y. Hao, S. Jandhyala, G. Mordi, J. Kim, L. Colombo, R. S. Ruoff, M. J. Kim, K. Cho, R. M. Wallace, and Y. J. Chabal, The Journal of Physical Chemistry C **117**(44), 23000–23008 (2013).

[24] C. W. Jang, J. H. Kim, J. M. Kim, D. H. Shin, S. Kim, and S. H. Choi, Nanotechnology **24**(40), 405301 (2013).

[25] J. N. Longchamp, C. Escher, and H. W. Fink, Journal of Vacuum Science & Technology B, Nanotechnology and Microelectronics: Materials, Processing, Measurement, and Phenomena **31**(2), 20605 (2013).

[26] A. M. Goossens, V. E. Calado, A. Barreiro, K. Watanabe, T. Taniguchi, and L. M. K. Vandersypen, Applied Physics Letters **100**(7), 73110 (2012).

[27] D. Ferrah, O. Renault, C. Petit-Etienne, H. Okuno, C. Berne, V. Bouchiat, and G. Cunge, Surface and Interface Analysis **48**(7), 451–455 (2016), SIA-15-0411.R1.

[28] H. Y. Nan, Z. H. Ni, J. Wang, Z. Zafar, Z. X. Shi, and Y. Y. Wang, Journal of Raman Spectroscopy **44**(7), 1018–1021 (2013).

[29] K. Kim, W. Regan, B. Geng, B. Alemn, B. M. Kessler, F. Wang, M. F. Crommie, and A. Zettl, physica status solidi (RRL) Rapid Research Letters **4**(11), 302–304 (2010).

[30] W. Gao and R. Huang, Journal of the Mechanics and Physics of Solids **66**, 42 – 58 (2014).

[31] F. C. Nix and D. MacNair, Phys. Rev. **60**(Oct), 597–605 (1941).

[32] O. L. Krivanek, M. F. Chisholm, V. Nicolosi, T. J. Pennycook, G. J. Corbin, N. Dellby, M. F. Murfitt, C. S. Own, Z. S. Szilagyi, M. P. Oxley, S. T. Pantelides, and S. J. Pennycook, Nature **464**(7288), 571–574 (2010).

[33] T. J. Booth, P. Blake, R. R. Nair, D. Jiang, E. W. Hill, U. Bangert, A. Bleloch, M. Gass, K. S. Novoselov, M. I. Katsnelson, and A. K. Geim, Nano Letters **8**(8), 2442–2446 (2008).